

Fluctuations of non-ergodic stochastic processes

G. George, L. Klochko, A.N. Semenov, J. Baschnagel, and J.P. Wittmer^a

Institut Charles Sadron, Université de Strasbourg & CNRS, 23 rue du Loess, 67034 Strasbourg Cedex, France

Received: date / Revised version: date

Abstract. We investigate the standard deviation $\delta v(\Delta t)$ of the variance $v[\mathbf{x}]$ of time series \mathbf{x} measured over a finite sampling time Δt focusing on non-ergodic systems where independent “configurations” c get trapped in meta-basins of a generalized phase space. It is thus relevant in which order averages over the configurations c and over time series k of a configuration c are performed. Three variances of $v[\mathbf{x}_{ck}]$ must be distinguished: the total variance $\delta v_{\text{tot}}^2 = \delta v_{\text{int}}^2 + \delta v_{\text{ext}}^2$ and its contributions δv_{int}^2 , the typical internal variance within the meta-basins, and δv_{ext}^2 , characterizing the dispersion between the different basins. We discuss simplifications for physical systems where the stochastic variable $x(t)$ is due to a density field averaged over a large system volume V . The relations are illustrated for the shear-stress fluctuations in quenched elastic networks and low-temperature glasses formed by polydisperse particles and free-standing polymer films. The different statistics of δv_{int} and δv_{ext} are manifested by their different system-size dependences.

1 Introduction

Expectation values \mathcal{O} and standard deviations $\delta\mathcal{O}$ of properties $\mathcal{O}[\mathbf{x}]$ averaged over finite time series \mathbf{x} of stochastic processes $x(t)$ [1, 2] are of relevance for a large variety of problems in scientific computing in general [1, 3] and especially in condensed matter [4, 5, 6, 7, 8, 9], material modeling [10, 11] and computational physics [12, 13]. We consider ensembles of equidistant time series

$$\mathbf{x} = \{x_i = x(t_i = i\delta t), i = 1, \dots, n_t\} \quad (1)$$

each containing n_t data entries x_i . The data sequence is taken from $t_1 = \delta t$ up to the “sampling time” $\Delta t = n_t\delta t$.¹ Examples of such time series obtained in a generalized phase space are sketched in Fig. 1. If the stochastic process $x(t)$ is *stationary* it may be characterized by means of the mean-square displacement

$$h(|t_i - t_j|) \equiv h_{i-j} \equiv \langle (x_i - x_j)^2 \rangle / 2, \quad (2)$$

of the data entries x_i . Note that $h(t) = c(0) - c(t)$ is closely related to the common autocorrelation function (ACF) $c(t) = \langle x(t)x(0) \rangle$ [7].² Ensemble averages $\langle \dots \rangle$ are commonly estimated by “*c*-averaging” over many independently prepared systems c , called here “configurations”. An example with $n_c = 3$ is given in Fig. 1. As in our previous work [14, 15], we shall focus on the “empirical

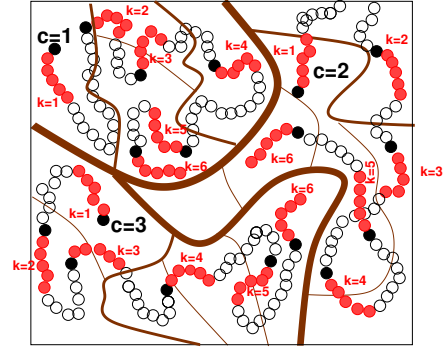


Fig. 1. Sketch of problem: Time series \mathbf{x} with $n_t = 6$ data entries x_i are marked by filled circles. The first entry $x_{i=1}$ is indicated by a dark filled circle. The open circles mark tempering steps between different time series k of each *independently* prepared “configuration” c . The solid lines mark barriers of different height in some phase space. We assume that the system is non-ergodic, i.e. the configurations c are permanently trapped in the meta-basins marked by the thickest lines.

sample variance”³

$$\mathcal{O}[\mathbf{x}] = v[\mathbf{x}] \equiv \frac{1}{n_t} \sum_{i=1}^{n_t} (x_i - \bar{x})^p \quad \text{with} \quad \bar{x} = \frac{1}{n_t} \sum_{i=1}^{n_t} x_i \quad (3)$$

and $p = 2$. Importantly, its expectation value $v = \langle v[\mathbf{x}] \rangle$ and variance $\delta v^2 = \langle (v[\mathbf{x}] - v)^2 \rangle$ are given by [14, 15]

$$v = \frac{2}{n_t^2} \sum_{i=1}^{n_t-1} (n_t - i) h_i \quad \text{and} \quad (4)$$

³ $v[\mathbf{x}]$ is defined without the usual “Bessel correction” [1]. See the discussion at the end of Sec. 2.1.

^a joachim.wittmer@ics-cnrs.unistra.fr

¹ The term “sampling time” is elsewhere often used for the time-interval δt between neighboring data points.

² The response function due to an externally applied “force” conjugated to x switched on at $t = 0$ is given within linear response by $h(t)$ [5].

$$\delta v^2 = \delta v_G^2[h] \equiv \frac{1}{2n_t^4} \sum_{i,j,k,l=1}^{n_t} g_{ijkl}^2 \quad \text{with} \quad (5)$$

$$g_{ijkl} \equiv (h_{i-j} + h_{k-l}) - (h_{i-l} + h_{j-k})$$

in terms of the ACF $h(t)$. While Eq. (4) is a direct consequence of the *stationarity* of the process, Eq. (5) assumes in addition that $x(t)$ is both *Gaussian* and *ergodic* [15]. Note that v and δv depend in general on the sampling time Δt of the time series.⁴

As sketched by the thickest solid lines in Fig. 1, if some large barriers are present in the generalized phase space the stochastic processes of independent configurations c must get trapped in meta-basins [29,30], at least for sampling times $\Delta t \ll \tau_\alpha$ with τ_α being the terminal relaxation time of the system. For such non-ergodic systems and for sufficiently large sampling times Δt (to be specified below) it was found [16,14,15] that $\delta v(\Delta t)$ becomes similar to a constant “non-ergodicity parameter” $\Delta_{\text{ne}} > 0$. δv thus differs from the rapidly decaying Gaussian prediction $\delta v_G \propto 1/\sqrt{\Delta t}$ [14,15]. To understand the observed discrepancy an *extended ensemble* of time series \mathbf{x}_{ck} is needed where for each configuration c one samples $n_k \gg 1$ time series k .⁵ k -averages and k -variances may then depend on the configuration c and it becomes relevant in which order c -averages over configurations c and k -averages over time series k of a given configuration c are performed. As described in Sec. 2.2, three variances must be distinguished:

- the standard “total variance” $\delta v_{\text{tot}}^2(\Delta t)$ obtained by lumping together the quantities $v[\mathbf{x}_{ck}]$ for all c and k ,
- the c -averaged “internal variance” $\delta v_{\text{int}}^2(\Delta t, n_k)$ of the meta-basins and
- the “external variance” $\delta v_{\text{ext}}^2(\Delta t, n_k)$ describing the dispersion between the different meta-basins.

δv_{tot} is commonly probed in previous computational work on fluctuations of v [16,17,18,19,20,14,15]. Importantly,

$$\delta v_{\text{tot}}^2(\Delta t) = \delta v_{\text{int}}^2(\Delta t, n_k) + \delta v_{\text{ext}}^2(\Delta t, n_k) \quad (6)$$

holds rigorously for large n_c and the n_k -dependence on the right-hand side becomes rapidly irrelevant with increasing n_k for non-ergodic systems. As will be discussed in Sec. 2.3, Eq. (6) can be simplified in many cases such that the total variance $\delta v_{\text{tot}}(\Delta t)$ can be traced back to the ACF $h(t)$ and the “non-ergodicity parameter” Δ_{ne} properly defined in Sec. 2.2. This leads especially to

$$\delta v_{\text{int}}(\Delta t) \simeq \sqrt{\tau_b/\Delta t} \quad \text{and} \quad \delta v_{\text{ext}}(\Delta t) \simeq \Delta_{\text{ne}} \quad (7)$$

for $\Delta t \gg \tau_b$ with τ_b being the typical basin relaxation time. Corroborating Ref. [15] it will be seen that system-size effects become rapidly irrelevant for physical systems

⁴ As seen by analyzing Eq. (5) [14,15], the standard deviation $\delta v(\Delta t)$ is small if $h(t)$ is essentially constant for $t \approx \Delta t$ but may become of order of $v(\Delta t)$ if $h(t)$ changes strongly for $t \approx \Delta t$.

⁵ The time series k may be obtained by first tempering the configuration c over a time interval Δt_{temp} larger than the basin relaxation time τ_b and by sampling then n_k time intervals Δt separated by constant spacer intervals $\Delta t_{\text{spac}} \gg \tau_b$.

where $x(t)$ is the average over a statistically uniform density field (Sec. 2.4).

Various relations and issues discussed theoretically in Sec. 2 are tested numerically in Sec. 4 for the fluctuations of the shear stresses in three strictly or in practice non-ergodic coarse-grained model systems described in Sec. 3. Temperature-effects are briefly discussed in Sec. 4.6, system-size effects in Sec. 4.7. The paper concludes in Sec. 5 with a summary and an outlook to future work. Appendix A presents further details on the power-law exponents describing the system-size dependence of v and Δ_{ne} , Appendix B the distribution of the frozen v_c for different configurations c .

2 Theoretical considerations

2.1 Some notations

To state compactly the expressions developed below it is useful to introduce a few notations. The l -average operator

$$\mathbf{E}^l \mathcal{O}_{lmn\dots} \equiv \frac{1}{n_l} \sum_{l=1}^{n_l} \mathcal{O}_{lmn\dots} \equiv \mathcal{O}_{mn\dots}(n_l) \quad (8)$$

takes a property $\mathcal{O}_{lmn\dots}$ depending possibly on several indices l, m, \dots and projects out the specified index l , i.e. the generated property $\mathcal{O}_{mn\dots}(n_l)$ does not depend any more on l , but it may depend on the upper bound n_l as marked by the argument. The latter dependence drops out for large n_l (formally $n_l \rightarrow \infty$) if $\mathcal{O}_{lmn\dots}$ is stationary or converges with respect to l . The l -variance operator \mathbf{V}^l is defined by

$$\mathbf{V}^l \mathcal{O}_{lmn\dots} \equiv \frac{1}{n_l} \sum_{l=1}^{n_l} (\mathcal{O}_{lmn\dots} - \mathbf{E}^l \mathcal{O}_{lmn\dots})^2. \quad (9)$$

Introducing the power-law operator $\mathbf{P}^\alpha \mathcal{O} \equiv \mathcal{O}^\alpha$, with the exponent $\alpha = 2$ being here the only relevant case, and using the standard commutator $[\mathbf{A}, \mathbf{B}] \equiv \mathbf{AB} - \mathbf{BA}$ for two operators \mathbf{A} and \mathbf{B} , the l -variance operator may be written $\mathbf{V}^l = [\mathbf{E}^l, \mathbf{P}^2]$. The result $\delta \mathcal{O}_{mn\dots}^2(n_l) = \mathbf{V}^l \mathcal{O}_{lmn\dots}$ of this operation on $\mathcal{O}_{lmn\dots}$ depends in general on the upper bound n_l . In the cases considered below $\delta \mathcal{O}_{mn\dots}^2(n_l)$ converges for large n_l and the n_l -dependency again drops out. This large- n_l limit is written

$$\delta \mathcal{O}_{mn\dots}^2(\dots) \equiv \lim_{n_l \rightarrow \infty} \delta \mathcal{O}_{mn\dots}^2(n_l, \dots) \quad (10)$$

where the dots \dots indicate possible additional variables. We emphasize finally that we have defined the l -variance operator \mathbf{V}^l , as above in Eq. (3) for $v[\mathbf{x}]$, as an “uncorrected biased sample variance” without the often used Bessel correction [1,13], i.e. we normalize with $1/n_l$ and not with $1/(n_l - 1)$. If the n_l contributions l are *uncorrelated* this can be readily shown to underestimate the asymptotic variance by a factor of $(n_l - 1)/n_l$ [13], i.e.

$$\delta \mathcal{O}_{mn\dots}^2(n_l, \dots) = \left(1 - \frac{1}{n_l}\right) \delta \mathcal{O}_{mn\dots}^2(\dots). \quad (11)$$

2.2 Extended ensembles of time series \mathbf{x}_{ck}

2.2.1 Ergodic systems

We remind first that in ergodic systems the terminal relaxation time τ_α is short relative to reasonable experimental or computational sampling times Δt , i.e. the time series can easily cross all barriers. One may thus either compute the averages $\mathbf{E}^c \mathcal{O}[\mathbf{x}_c]$ and $\mathbf{V}^c \mathcal{O}[\mathbf{x}_c]$ over n_c independent configurations c (with $n_k = 1$) or the averages $\mathbf{E}^k \mathcal{O}[\mathbf{x}_k]$ and $\mathbf{V}^k \mathcal{O}[\mathbf{x}_k]$ over $n_k \gg 1$ different time series k of one long trajectory (with $n_c = 1$). Hence,

$$\mathbf{E}^c \mathcal{O}[\mathbf{x}_c] \simeq \mathbf{E}^k \mathcal{O}[\mathbf{x}_k] \text{ and } \mathbf{V}^c \mathcal{O}[\mathbf{x}_c] \simeq \mathbf{V}^k \mathcal{O}[\mathbf{x}_k] \quad (12)$$

holds for sufficiently large n_c and n_k . Importantly, it is sufficient for ergodic systems to characterize a time series \mathbf{x} by *one* index. We come back to ergodic systems in Sec. 2.2.9.

2.2.2 Non-Ergodic systems

Let us focus now on strictly non-ergodic systems with infinite terminal relaxation times τ_α for the transitions between the meta-basins. We characterize a time series \mathbf{x}_{ck} by the *two* discrete indices c and k with $1 \leq c \leq n_c$ and $1 \leq k \leq n_k$. As shown in Fig. 1, the index c stands for the “configurations” (or set-ups) generated by completely independent preparation histories for the system probed, the index k for subsets of length n_t of a much larger trajectory generated for a fixed configuration c . The central point is now that

$$\mathcal{O}_c(\Delta t, n_k) \equiv \mathbf{E}^k \mathcal{O}[\mathbf{x}_{ck}] \text{ and} \quad (13)$$

$$\delta \mathcal{O}_c^2(\Delta t, n_k) \equiv \mathbf{V}^k \mathcal{O}[\mathbf{x}_{ck}] \quad (14)$$

do depend in general not only on the sampling time $\Delta t = n_t \delta t$ of the time series and the number n_k of time series probed but crucially also on c — even for arbitrarily large n_t and n_k — since the “ c -trajectory” of each configuration c is trapped (Fig. 1). For $\Delta t \gg \tau_b$ much larger than the typical basin relaxation time τ_b the Δt -dependence of $\mathcal{O}_c(\Delta t, n_k)$ drops out and $\delta \mathcal{O}_c(\Delta t, n_k) \propto 1/\sqrt{\Delta t/\tau_b}$ since we average over $\Delta t/\tau_b$ independent subintervals. Moreover, the n_k -dependence must disappear if $n_k \gg 1$ and the c -trajectory has completely explored the basin. Assuming that after each measurement interval of length Δt a spacer (tempering) step of length Δt_{spac} follows, as marked by the open circles in Fig. 1, this happens for c -trajectories of total length $\Delta t_{\text{max}} \equiv n_k \times (\Delta t + \Delta t_{\text{spac}})$ with

$$\tau_b \ll \Delta t \ll \Delta t_{\text{max}} \ll \tau_\alpha. \quad (15)$$

The first inequality implies that the sampling is ergodic within the metabasin (that’s why, the metabasin is sometimes said to be an “ergodic component”), while the last inequality states the ergodicity breaking of the system.

2.2.3 Commuting and non-commuting operators

Since $[\mathbf{E}^c, \mathbf{E}^k] = 0$ we may write quite generally

$$\mathbf{E}^c \mathbf{E}^k \mathcal{O}[\mathbf{x}_{ck}] = \mathbf{E}^k \mathbf{E}^c \mathcal{O}[\mathbf{x}_{ck}] = \mathbf{E}^l \mathcal{O}[\mathbf{x}_l] = \mathcal{O}, \quad (16)$$

i.e. the two indices c and k can be lumped together to one index l . Averages of this type are called “simple averages”. For instance, the average variance $v = \mathbf{E}^c \mathbf{E}^k v[\mathbf{x}_{ck}] = \mathbf{E}^l v[\mathbf{x}_l]$ is a simple average. At variance to this in general

$$[\mathbf{E}^c, \mathbf{V}^k] \neq 0 \text{ or } [\mathbf{V}^c, \mathbf{E}^k] \neq 0 \text{ if } n_k > 1. \quad (17)$$

Two operators of this type thus cannot be commuted and the indices c and k cannot be exchanged or lumped together.

2.2.4 Different variances

We define now in general terms the three variances mentioned in the Introduction:

$$\delta \mathcal{O}_{\text{tot}}^2(\Delta t, n_c, n_k) \equiv [\mathbf{E}^c \mathbf{E}^k, \mathbf{P}^2] \mathcal{O}[\mathbf{x}_{ck}] \quad (18)$$

$$\delta \mathcal{O}_{\text{int}}^2(\Delta t, n_c, n_k) \equiv \mathbf{E}^c \delta \mathcal{O}_c^2 = \mathbf{E}^c \mathbf{V}^k \mathcal{O}[\mathbf{x}_{ck}] \quad (19)$$

$$\delta \mathcal{O}_{\text{ext}}^2(\Delta t, n_c, n_k) \equiv \mathbf{V}^c \mathcal{O}_c = \mathbf{V}^c \mathbf{E}^k \mathcal{O}[\mathbf{x}_{ck}]. \quad (20)$$

The indicated dependencies on Δt , n_c and n_k will be discussed in detail below (Sec. 2.2.5-2.2.8). Let us stress first that the “total variance” $\delta \mathcal{O}_{\text{tot}}^2$ is a simple average, i.e. all time series \mathbf{x}_{ck} can be lumped together:

$$\delta \mathcal{O}_{\text{tot}}^2 = \mathbf{V}^l \mathcal{O}[\mathbf{x}_l] = [\mathbf{E}^l, \mathbf{P}^2] \mathcal{O}[\mathbf{x}_l]. \quad (21)$$

Importantly, the expectation value of $\delta \mathcal{O}_{\text{tot}}$ for $n_c \rightarrow \infty$ is strictly n_k -independent and may be also computed by using only *one* time series for each configuration ($n_k = 1$). $\delta \mathcal{O}_{\text{tot}}^2$ is thus the standard commonly computed variance [16, 17, 18, 19, 20, 14, 15]. The “internal variance” $\delta \mathcal{O}_{\text{int}}^2$ and the “external variance” $\delta \mathcal{O}_{\text{ext}}^2$ are different types of observables since Eq. (17) holds, i.e. c and k cannot be lumped together. Note also that $\delta \mathcal{O}_{\text{int}}$ and $\delta \mathcal{O}_{\text{ext}}$ do depend on n_k even for $n_c \rightarrow \infty$ and that $\delta \mathcal{O}_{\text{ext}}$ vanishes if all \mathcal{O}_c are identical. Using the identity

$$\begin{aligned} \mathbf{V}^l &= [\mathbf{E}^l, \mathbf{P}^2] = [\mathbf{E}^c \mathbf{E}^k, \mathbf{P}^2] \\ &= \mathbf{E}^c \mathbf{E}^k \mathbf{P}^2 - \mathbf{E}^c \mathbf{P}^2 \mathbf{E}^k + \mathbf{E}^c \mathbf{P}^2 \mathbf{E}^k - \mathbf{P}^2 \mathbf{E}^c \mathbf{E}^k \\ &= \mathbf{E}^c \mathbf{V}^k + \mathbf{V}^c \mathbf{E}^k \end{aligned} \quad (22)$$

$\delta \mathcal{O}_{\text{tot}}^2$ can be *exactly* decomposed as the sum

$$\begin{aligned} \delta \mathcal{O}_{\text{tot}}^2(\Delta t, n_c, n_k) &= \delta \mathcal{O}_{\text{int}}^2(\Delta t, n_c, n_k) \\ &\quad + \delta \mathcal{O}_{\text{ext}}^2(\Delta t, n_c, n_k) \end{aligned} \quad (23)$$

of the two *independent* variances $\delta \mathcal{O}_{\text{int}}^2$ and $\delta \mathcal{O}_{\text{ext}}^2$. Details of both contributions $\delta \mathcal{O}_{\text{int}}$ and $\delta \mathcal{O}_{\text{ext}}$ depend on the properties of the considered stochastic process $x(t)$ and the functional $\mathcal{O}[\mathbf{x}]$ considered. However, the following fairly general statements can be made.

2.2.5 n_c -dependences

Let us define the large- n_c limits

$$\delta\mathcal{O}_{\text{ext}}(\Delta t, n_k) \equiv \lim_{n_c \rightarrow \infty} \delta\mathcal{O}_{\text{ext}}(\Delta t, n_k, n_c) \quad (24)$$

$$\begin{aligned} \delta\mathcal{O}_{\text{tot}}(\Delta t) &= \delta\mathcal{O}_{\text{tot}}(\Delta t, n_k) \\ &\equiv \lim_{n_c \rightarrow \infty} \delta\mathcal{O}_{\text{tot}}(\Delta t, n_k, n_c) \end{aligned} \quad (25)$$

where the n_k -dependence of $\delta\mathcal{O}_{\text{tot}}$ does not emerge as already stated below Eq. (21). As all the configurations c are assumed to be strictly independent, $\delta\mathcal{O}_{\text{int}}$ does not depend on n_c , i.e.

$$\delta\mathcal{O}_{\text{int}}(\Delta t, n_c, n_k) = \delta\mathcal{O}_{\text{int}}(\Delta t, n_k), \text{ and} \quad (26)$$

$$\delta\mathcal{O}_{\text{ext}}^2(\Delta t, n_c, n_k) = \left(1 - \frac{1}{n_c}\right) \delta\mathcal{O}_{\text{ext}}^2(\Delta t, n_k) \quad (27)$$

where we have used the general relation Eq. (11). Using Eq. (23) this implies

$$\delta\mathcal{O}_{\text{tot}}^2(\Delta t, n_c, n_k) = \delta\mathcal{O}_{\text{tot}}^2(\Delta t) - \frac{\delta\mathcal{O}_{\text{ext}}^2(\Delta t, n_k)}{n_c}. \quad (28)$$

If not emphasized otherwise, we assume below that n_c is large, say at least $n_c \approx 100$, and the stated n_c -dependences thus become irrelevant.

2.2.6 n_k -dependences

While $\delta\mathcal{O}_{\text{int}}$ and $\delta\mathcal{O}_{\text{ext}}$ depend in principle on n_k , this dependence must drop out for large n_k if $\Delta t_{\text{max}} \gg \tau_b$ as noted in Sec. 2.2.4. It is therefore useful to define:

$$\delta\mathcal{O}_{\text{int}}(\Delta t) \equiv \lim_{n_k \rightarrow \infty} \delta\mathcal{O}_{\text{int}}(\Delta t, n_k), \quad (29)$$

$$\delta\mathcal{O}_{\text{ext}}(\Delta t) \equiv \lim_{n_k \rightarrow \infty} \delta\mathcal{O}_{\text{ext}}(\Delta t, n_k). \quad (30)$$

Note also that $\delta\mathcal{O}_{\text{int}}(\Delta t, n_k) = 0$ and $\delta\mathcal{O}_{\text{ext}}(\Delta t, n_k) = \delta\mathcal{O}_{\text{tot}}(\Delta t)$ in the opposite limit, $n_k = 1$. In what follows we assume that the spacer time intervals Δt_{spac} between the measured time series k of a configuration c is large, i.e. either $\Delta t_{\text{spac}} \gg \tau_b$ or $\Delta t_{\text{spac}} + \Delta t \gg \tau_b$. In this case all n_k time series for each configuration must be virtually independent (albeit constraint to be in the same basin). Therefore,

$$\delta\mathcal{O}_{\text{int}}^2(\Delta t, n_k) \simeq \left(1 - \frac{1}{n_k}\right) \delta\mathcal{O}_{\text{int}}^2(\Delta t) \quad (31)$$

providing the n_k -dependence of $\delta\mathcal{O}_{\text{int}}$ for sufficiently large Δt_{spac} . Using Eq. (23) both for finite n_k and for $n_k \rightarrow \infty$ and the fact that $\delta\mathcal{O}_{\text{tot}}(\Delta t, n_k) = \delta\mathcal{O}_{\text{tot}}(\Delta t)$, i.e. $\delta\mathcal{O}_{\text{tot}}$ does not depend on n_k for large n_c , we get

$$\delta\mathcal{O}_{\text{ext}}^2(\Delta t, n_k) \simeq \delta\mathcal{O}_{\text{ext}}^2(\Delta t) + \frac{1}{n_k} \delta\mathcal{O}_{\text{int}}^2(\Delta t) \quad (32)$$

for $\Delta t_{\text{spac}} \gg \tau_b$ and $n_c \rightarrow \infty$. $\delta\mathcal{O}_{\text{ext}}(\Delta t, n_k)$ thus depends on n_k and $\delta\mathcal{O}_{\text{ext}}(\Delta t)$ and, interestingly, also on $\delta\mathcal{O}_{\text{int}}(\Delta t)$.

2.2.7 Total variance $\delta v_{\text{tot}}^2(\Delta t, n_c, n_k)$

Using Eqs. (28, 32) the total variance, Eq. (23), can be written for finite n_c as

$$\begin{aligned} \delta\mathcal{O}_{\text{tot}}^2(\Delta t, n_c, n_k) &\simeq \left(1 - \frac{1}{n_k}\right) \delta\mathcal{O}_{\text{int}}^2(\Delta t) \\ &+ \left(1 - \frac{1}{n_c}\right) \left(\delta\mathcal{O}_{\text{ext}}^2(\Delta t) + \frac{1}{n_k} \delta\mathcal{O}_{\text{int}}^2(\Delta t)\right). \end{aligned} \quad (33)$$

The latter equation is valid for $\Delta t + \Delta t_{\text{spac}} \gg \tau_b$ and $\Delta t_{\text{max}} \ll \tau_\alpha$. It shows explicitly how $\delta\mathcal{O}_{\text{tot}}^2$ depends on the number of configurations n_c and the number of time series n_k for each c . For $n_c \rightarrow \infty$ Eq. (33) simplifies to

$$\begin{aligned} \delta\mathcal{O}_{\text{tot}}^2(\Delta t, n_c, n_k) &\rightarrow \delta\mathcal{O}_{\text{tot}}^2(\Delta t) \\ &= \delta\mathcal{O}_{\text{int}}^2(\Delta t) + \delta\mathcal{O}_{\text{ext}}^2(\Delta t) \end{aligned} \quad (34)$$

i.e. as expected from Sec. 2.2.4 not only the n_c -dependence but also the n_k -dependence drops out.

2.2.8 Large- Δt limit ($\Delta t \gg \tau_b$)

Here and below we return to real non-ergodic systems with very large but finite terminal relaxation times τ_α . Without additional assumptions it is also clear that

$$\delta\mathcal{O}_{\text{int}} \propto 1/\sqrt{\Delta t/\tau_b}, \quad \delta\mathcal{O}_{\text{ext}}(\Delta t) \simeq \Delta_{\text{ne}} = \text{const}, \quad (35)$$

for $\tau_\alpha \gg \Delta t \gg \tau_b$ with the ‘‘non-ergodicity parameter’’ Δ_{ne} being defined by the finite limit of $\delta\mathcal{O}_{\text{ext}}$ at large Δt

$$\Delta_{\text{ne}} \equiv \lim_{\Delta t/\tau_b \rightarrow \infty} \delta\mathcal{O}_{\text{ext}}(\Delta t, n_k). \quad (36)$$

This is equivalent to the large- Δt limit of $\delta\mathcal{O}_{\text{tot}}(\Delta t)$ since the n_k -dependence of $\delta\mathcal{O}_{\text{ext}}$ drops out for large Δt . (The last statement may be also seen from Eq. (32).) As already noted, the first asymptotic law in Eq. (35) is a consequence of the $\Delta t/\tau_b$ uncorrelated subintervals for each c -trajectory while the second limit is merely a consequence of the $\mathcal{O}_c(\Delta t)$ becoming constant. Equation (35) implies that $\delta\mathcal{O}_{\text{tot}}$ must become

$$\delta\mathcal{O}_{\text{tot}} \rightarrow \delta\mathcal{O}_{\text{ext}} \approx \Delta_{\text{ne}} \text{ for } \Delta t \gg \tau_{\text{ne}} \gg \tau_b. \quad (37)$$

Note that the crossover to the Δ_{ne} -dominated regime occurs at an additional time scale τ_{ne} . Operationally, this ‘‘non-ergodicity time’’ τ_{ne} may be defined as

$$\delta\mathcal{O}_{\text{int}}(\Delta t \stackrel{!}{=} \tau_{\text{ne}}) = \Delta_{\text{ne}}. \quad (38)$$

Δ_{ne} does not depend on n_k , being equivalently the large- Δt limit of either $\delta\mathcal{O}_{\text{ext}}(\Delta t, n_k)$ or $\delta\mathcal{O}_{\text{tot}}(\Delta t)$, the latter simple average being strictly n_k -independent ($n_c \rightarrow \infty$). Coming back to Eq. (32) and using Eq. (36) one sees that

$$\delta\mathcal{O}_{\text{ext}}^2(\Delta t, n_k) \simeq \Delta_{\text{ne}}^2 + \frac{1}{n_k} \delta\mathcal{O}_{\text{int}}^2(\Delta t) \text{ and} \quad (39)$$

$$\delta\mathcal{O}_{\text{tot}}^2(\Delta t) \simeq \Delta_{\text{ne}}^2 + \delta\mathcal{O}_{\text{int}}^2(\Delta t) \quad (40)$$

for $\tau_\alpha \gg \Delta t \gg \tau_b$ and $n_c \rightarrow \infty$.

2.2.9 Back to ergodic systems

Let us finally assume that the terminal relaxation time τ_α is shorter than the sampling time, $\Delta t \gg \tau_\alpha$. In this ergodic limit all trajectories become statistically equivalent, i.e. $\delta\mathcal{O}_{\text{ext}}(\Delta t) = 0$ (cf. Eq. (30)). Following Eq. (27) and Eq. (32) we have

$$\delta\mathcal{O}_{\text{ext}}^2(\Delta t, n_c, n_k) = \left(1 - \frac{1}{n_c}\right) \frac{1}{n_k} \delta\mathcal{O}_{\text{int}}^2(\Delta t) \quad (41)$$

and using Eq. (26) and Eq. (31) we get

$$\delta\mathcal{O}_{\text{int}}^2(\Delta t, n_c, n_k) = \left(1 - \frac{1}{n_k}\right) \delta\mathcal{O}_{\text{int}}^2(\Delta t). \quad (42)$$

This implies by means of Eq. (23) or, equivalently, using Eq. (33)

$$\delta\mathcal{O}_{\text{tot}}^2(\Delta t, n_c, n_k) = \left(1 - \frac{1}{n_k n_c}\right) \delta\mathcal{O}_{\text{int}}^2(\Delta t). \quad (43)$$

For either $n_c \rightarrow \infty$ or $n_k \rightarrow \infty$ the latter relation yields finally

$$\delta\mathcal{O}_{\text{tot}}(\Delta t, n_c, n_k) \rightarrow \delta\mathcal{O}_{\text{tot}}(\Delta t) = \delta\mathcal{O}_{\text{int}}(\Delta t) \quad (44)$$

which is similar to the second relation stated in Eq. (12).

2.3 Properties related to $\mathcal{O}[\mathbf{x}] = v[\mathbf{x}]$

From now on we shall focus on $\mathcal{O}[\mathbf{x}] = v[\mathbf{x}]$, Eq. (3), for $p = 2$. Our key results Eq. (6) and Eq. (7) follow directly from the more general relations Eq. (23) and Eq. (35). Assuming an *ergodic* Gaussian process we have expressed $\delta v(\Delta t)$ by the functional $\delta v_G[h]$ in terms of the ACF h , Eq. (5). Numerically better behaved equivalent reformulations are discussed in Ref. [15]. We make now the additional physical assumption that

after sufficient tempering the stochastic process of each configuration c in its meta-basin is both stationary and Gaussian.

This implies that for $\tau_b \ll \Delta t_{\text{max}} \ll \tau_\alpha$ Eq. (5) may hold for each basin separately.⁶ i.e. δv_c is given by $\delta v_G[h_c]$ expressed in terms of the corresponding ACF h_c of the basin instead of its c -average $h = \mathbf{E}^c h_c$. Unfortunately, h_c is not known in general (at least not to sufficient accuracy), but rather h . Since Eq. (5) corresponds to products of h_c , it is a ‘‘mean-field type’’ approximation to replace h_c by its c -average h . This technical assumption becomes strictly valid for large systems, $V \rightarrow \infty$, since fluctuations of the ACF vanish in this limit. Within the above physical assumption and the additional technical approximation one thus expects after a final c -averaging

$$\delta v_{\text{int}}(\Delta t) \approx \delta v_G[h] \text{ with } h = \mathbf{E}^c h_c \quad (45)$$

⁶ This assumption also holds for $\Delta t \gg \tau_\alpha$ for a finite terminal relaxation time τ_α associated with the transitions between the meta-basins. Note that the systems is ergodic in the second regime.

to hold for all Δt . Whether this approximation is good enough must be checked for each case. Note that neither $\delta v_G[h]$ nor $\delta v_{\text{int}}(\Delta t)$ do depend (explicitly) on n_c or n_k , i.e. Eq. (45) only holds for $\delta v_{\text{int}}(\Delta t, n_k)$ with sufficiently large n_k . Fortunately, due to Eq. (31)

$$\delta v_{\text{int}}(\Delta t) \simeq \delta v_{\text{int}}(\Delta t, n_k) / \sqrt{1 - 1/n_k}, \quad (46)$$

i.e. by computing even a small number n_k of time series the asymptotic limit $\delta v_{\text{int}}(\Delta t)$ may be obtained. The relations Eq. (34), Eq. (36) and Eq. (45) suggest the simple interpolation

$$\delta v_{\text{tot}}(\Delta t) \approx \sqrt{\delta v_G^2[h] + \Delta_{\text{ne}}^2} \quad (47)$$

stating that δv_{tot} is essentially given by $h(t)$ plus an additional constant Δ_{ne} .

2.4 General system-size effects

The stochastic processes of many systems are to a good approximation Gaussian since the data entries $x_i = \mathbf{E}^m x_{im}$ are averages over $n_m \gg 1$ microscopic contributions x_{im} and the central limit theorem applies [2]. (These contributions are often unknown and experimentally inaccessible.) It is assumed here that the system is split in n_m quasi-independent microcells, n_m is proportional to the volume V , and x_{im} comes from the m -th microcell. Albeit the x_{im} may be correlated, i.e. they may not all fluctuate independently, the fluctuations of the x_i commonly decrease with increasing n_m . As a consequence, δv_{int} and δv_{ext} generally decrease with the system size. Assuming scale-free correlations one may write [15]

$$\delta v_{\text{int}}(\Delta t) \propto 1/n_m^{\hat{\gamma}_{\text{int}}} \text{ and } \delta v_{\text{ext}}(\Delta t) \propto 1/n_m^{\hat{\gamma}_{\text{ext}}} \quad (48)$$

introducing the two phenomenological exponents $\hat{\gamma}_{\text{int}}$ and $\hat{\gamma}_{\text{ext}}$. If the stochastic processes of all basins are Gaussian the same exponent $\hat{\gamma}_{\text{int}}$ must hold for $\delta v_G[h] \approx \delta v_{\text{int}}(\Delta t)$, Eq. (45). In turn due to Eq. (5) this implies the same exponent for $h(t)$ and then due to the stationarity relation Eq. (4) also for $v(\Delta t)$. Due to the definition Eq. (36) the same exponent $\hat{\gamma}_{\text{ext}}$ must hold for $\delta v_{\text{ext}}(\Delta t)$ and Δ_{ne} .

As reminded in Appendix A it is readily seen that $\hat{\gamma}_{\text{int}} = 1$ and $\hat{\gamma}_{\text{ext}} = 3/2$ for strictly uncorrelated variables x_{im} . The uncorrelated reference with $\hat{\gamma}_{\text{int}} = 1$ is often included into the definition of the data entries by rescaling $x_i \Rightarrow \sqrt{n_m} x_i$. Hence, $\hat{\gamma}_{\text{int}} \Rightarrow \gamma_{\text{int}} \equiv \hat{\gamma}_{\text{int}} - 1$ and $\hat{\gamma}_{\text{ext}} \Rightarrow \gamma_{\text{ext}} \equiv \hat{\gamma}_{\text{ext}} - 1$ in the above relations, i.e.

$$\gamma_{\text{int}} = 0 \text{ and } \gamma_{\text{ext}} = 1/2 \quad (49)$$

for rescaled uncorrelated variables x_{im} . Using the definition of the non-ergodicity time τ_{ne} , Eq. (38), and the asymptotic limit Eq. (35) it is seen that

$$\tau_{\text{ne}} \propto n_m^{2(\gamma_{\text{ext}} - \gamma_{\text{int}})} \text{ for } \tau_{\text{ne}} \gg \tau_b. \quad (50)$$

For uncorrelated microcells we have $\tau_{\text{ne}} \propto n_m$ and, moreover, $h(t)$ and thus τ_b are n_m -independent, i.e. the condition $\tau_{\text{ne}} \gg \tau_b$ becomes rapidly valid.

2.5 Fields of intensive thermodynamic variables

Up to now our description of ergodic and non-ergodic stochastic processes has remained deliberately general and we have specifically avoided the notions and assumptions of thermodynamics and statistical physics [4,10,11]. We shall now assume that each c -trajectory in its meta-basin is not only stationary and Gaussian but, moreover, at thermal equilibrium albeit under the (not necessarily known) constraints imposed to the basin.

We focus below on (instantaneous) intensive thermodynamic variables $\hat{\sigma}$ (other than the temperature) which are d -dimensional volume averages

$$\hat{\sigma}(t) = \frac{1}{V} \int d\mathbf{r} \hat{\sigma}_{\mathbf{r}}(t) \quad (51)$$

over (instantaneous) fields $\hat{\sigma}_{\mathbf{r}}(t)$ of local contributions (of same dimension). For such generic fields n_m corresponds to the number of local volume elements dV computed. Following the rescaling convention mentioned in Sec. 2.4 the stochastic process is obtained by rescaling

$$\hat{\sigma}(t) \Rightarrow x(t) \equiv \sqrt{\beta V} \hat{\sigma}(t) \quad (52)$$

with $\beta = 1/k_B T$ being the inverse temperature. For density fields $\hat{\sigma}_{\mathbf{r}}$ characterized by a finite correlation length ξ this rescaling leads to the same exponents $\gamma_{\text{int}} = 0$ and $\gamma_{\text{ext}} = 1/2$ as for completely uncorrelated microscopic variables. This assumes that $\xi^d \ll V$ and that ξ is V -independent.

Importantly, $\gamma_{\text{int}} = 0$ must even hold for systems with some long-range correlations if standard thermostatics can be used for each basin. To see this let us first note that the large- Δt limit v_c of $v_c(\Delta t)$ is equivalent to the thermodynamically averaged variance of $x(t)$ for the basin.⁷ Using the standard relation for the fluctuation of intensive thermodynamic variables [4,21] this implies that v_c does not depend explicitly on V .⁸ This suggests that $\gamma_{\text{int}} = 0$ not only holds for v_c but also for $v_c(\Delta t)$ and $v(\Delta t) = \mathbf{E}^c v_c(\Delta t)$ and in turn using Eq. (4) also for $h_c(t)$ and $h(t) = \mathbf{E}^c h_c(t)$, using Eq. (5) also for $\delta v_G[h_c]$ and $\delta v_G[h]$ and finally using Eq. (45) also for $\delta v_{\text{int}}(\Delta t)$. Interestingly, the same reasoning *cannot* be made for γ_{ext} , i.e. it is possible that for quenched configurations with long-ranged correlations $\gamma_{\text{int}} = 0$ holds but not $\gamma_{\text{ext}} = 1/2$.

3 Models and technical details

3.1 Coarse-grained models

Various issues discussed theoretically in Sec. 2 will be tested in Sec. 4 for the fluctuating shear stresses $\hat{\sigma}(t)$ measured in computational amorphous solids. We present numerical results obtained by means of molecular dynamics

⁷ The stochastic process is ergodic within the basin.

⁸ Albeit v_c depends on whether the average intensive variable σ of the meta-basin is imposed or its conjugated extensive variable in both cases v_c does not depend on V . See Ref. [22] or Sec. II.A of Ref. [21] for details.

(MD) and Monte Carlo (MC) simulations [12,13] of three coarse-grained model systems:

- quenched elastic networks of repulsive spheres in $d = 2$ dimensions connected by harmonic springs. The networks are created by means of the “transient self-assembled network” (TSANET) model [17,15] where springs break and recombine locally with an MC hopping frequency ν changing the connectivity matrix of the network. The latter MC moves are switched off ($\nu = 0$) for all configurations considered in the present work. Standard MD simulation with a strong Langevin thermostat [12] moves the particles effectively by overdamped motion through the phase space.
- dense polydisperse Lennard-Jones (pLJ) particles in $d = 2$ dimensions [23,24,21,15]. The configurations are first equilibrated for different temperatures at an imposed average pressure $P = 2$ using in addition to standard local MC moves of the particles [13,21] swap MC moves [25] exchanging pairs of particles. We then switch off the swap MC moves and the barostat. Note that each configuration has then a slightly different constant volume V .
- thin free-standing polymer films suspended parallel to the (x, y) -plane [20,15] computed by straight-forward MD simulation of a widely used bead-spring model [26]. The films contain $M = 768$ monodisperse chains of length $N = 16$, i.e. in total $n = 12288$ monomers, in a periodic box of lateral box size $L = 23.5$.

A brief presentation of the salient features of each model and the quench protocols used to create the configurations considered in the present work may be found in Ref. [15].

3.2 Parameters and some properties

Boltzmann’s constant k_B , the typical size of the particles (beads) and the particle mass of all models are set to unity and Lennard-Jones (LJ) units [12] are used throughout this work. Time is measured for the pLJ particles in units of MC cycles of the local MC hopping moves of the beads. Periodic boundary conditions [12,13] are used for all systems. The temperature T and the particle number n are imposed. Some key properties such as the main simulation method, the spatial dimension d , the linear dimension of the simulation box L , the volume V , the standard particle number n , the working temperature T or the pressure P are summarized in Table 1.⁹ The number density $\rho = n/V$ is always close to unity. The working temperature T of the pLJ particles and the polymer films are both well below the indicated glass transition temperature T_g . (There is no glass transition for the TSANET model.) The terminal (liquid) relaxation time τ_α [7,9] of all models is

⁹ The film volume is $V = L^2 H$ with H being the film height determined from the density profile using a Gibbs dividing surface construction [20]. Since the stress tensor vanishes outside the films, the average vertical normal stress must also vanish for all z -planes within the films. The pressure P indicated for the films in Table 1 refers to the normal tangential stresses.

property	symbol	TSANET	pLJ	films
main simulation method	-	MD	MC	MD
spatial dimension	d	2	2	3
linear simulation box size	L	100	≈ 103.3	23.5
system volume	V	L^2	L^2	L^2H
particle number	n	10000	10000	12288
number density	ρ	1	≈ 0.94	≈ 1.00
pressure	P	1.7	2.0	-1.0
temperature	T	1	0.2	0.05
glass transition temperature	T_g	none	≈ 0.26	≈ 0.36
number of configurations	n_c	100	100	100
maximum sampling time	Δt_{\max}	10^5	10^7	10^5
measurement time increment	δt	0.01	1	0.05
plateau of $v(\Delta t)$	v_p	15.3	17.1	≈ 83
basin relaxation time	τ_b	10	2000	1
non-ergodicity time	τ_{ne}	4200	200000	800
non-ergodicity parameter	Δ_{ne}	0.16	0.25	1.13
volume exponent for δv_{int}	γ_{int}	≈ 0	≈ 0	-
volume exponent for δv_{ext}	γ_{ext}	≈ 0.5	≈ 0.44	-

Table 1. Parameters and properties of the models investigated: general simulation method, spatial dimension d , linear size (length) L of periodic simulation box, system volume V , imposed particle number n , number density $\rho = n/V$, average normal pressure P , imposed temperature T , glass transition temperature T_g for the pLJ particles and the freestanding polymer films, number of independent configurations n_c , maximum sampling time Δt_{\max} for each trajectory, time increment δt between the measured observables, plateau value v_p of variance $v(\Delta t)$, relaxation time of basin τ_b (Fig. 3), non-ergodicity time τ_{ne} (Fig. 5), non-ergodicity parameter Δ_{ne} (Fig. 3) and system-size exponents γ_{int} and γ_{ext} (Fig. 9).

either (by construction) infinite for the quenched elastic networks of the TSANET model or many orders of magnitude larger than the maximum sampling time Δt_{\max} used for the production runs of each of the n_c independent configurations of the ensemble. The relaxation time τ_b of the meta-basins may be obtained from the leveling-off of $v(\Delta t)$ as shown in Sec. 4.2. The non-ergodicity parameter Δ_{ne} is determined equivalently from the large- Δt limit of δv_{tot} or δv_{ext} and τ_{ne} by setting $\delta v_{\text{int}}(\Delta t = \tau_{ne}) = \Delta_{ne}$, Eq. (38). Additional particle numbers n are considered for the pLJ particles ($n = 100, 200, 500, 1000, 2000, 50000$ and 10000) in Sec. 4.7 where we discuss system-size effects. We briefly report in Sec. 4.6 on preliminary work on temperature effects for the same model where data for $T = 0.19, 0.2, 0.25, 0.3$ and 0.4 are presented.

3.3 Observables and data handling

The only observable relevant for Sec. 4 is the excess contribution $\hat{\sigma}$ to the instantaneous shear stress in the xy -plane. See Ref. [15] for other related properties. Measurements are performed every δt as indicated in Table 1.¹⁰ Assuming a pairwise central conservative potential $\sum_l u(r_l)$ with r_l being the distance between a pair of monomers l , the shear stress is given by the off-diagonal contribution to

the Kirkwood stress tensor [12, 11]

$$\hat{\sigma}(t) = \frac{1}{V} \sum_l r_l u'(r_l) n_{l,x} n_{l,y} \quad (53)$$

with $n_l = r_l/r_l$ being the normalized distance vector. The stochastic process $x(t)$ is obtained using Eq. (52). With this rescaling $v[\mathbf{x}]$, Eq. (3), characterizes the empirical shear-stress fluctuations of the time series and the expectation value $v(\Delta t)$ is equivalent to the shear-stress fluctuation modulus $\mu_F(\Delta t)$ considered in previous publications on the stress-fluctuation formalism for elastic moduli [21, 17, 18, 19, 20, 14, 15]. The total standard deviation $\delta v_{\text{tot}}(\Delta t)$ was called $\delta \mu_F$ in Ref. [14] and δv in Ref. [15]. For clarity we keep below the notations introduced in Sec. 1 and Sec. 2.

As indicated in Table 1 we prepare for each considered model $n_c = 100$ independent configurations c . This allows to probe all properties accurately. For each configuration c we compute and store *one* long trajectory with $\Delta t_{\max}/\delta t \approx 10^7$ data entries. Since we want to investigate the dependence of various properties on the sampling time Δt we probe for each Δt_{\max} -trajectory n_k equally spaced subintervals k of length $\Delta t \leq \Delta t_{\max}$ with $n_t = \Delta t/\delta t$ entries. Most of the reported results have been obtained for discrete n_k corresponding to $\Delta t = \Delta t_{\max}/n_k$, i.e. n_k and Δt are coupled and all sampled data entries are used ($\Delta t_{\text{spac}} = 0$). As a shorthand we mark these data sets by “ $n_k \propto 1/\Delta t$ ”. We remind that $\delta v_{\text{int}} \rightarrow 0$ and $\delta v_{\text{ext}} \rightarrow \delta v_{\text{tot}}$ for $n_k \rightarrow 1$ (Sec. 2.2). This limit becomes relevant for $\Delta t \approx \Delta t_{\max}$. We have compared these results with averages taken at fixed constant n_k . This is done to show that δv_{int}

¹⁰ The standard deviations may depend in addition on the time increment δt used to sample the stochastic process [14]. For each model system one unique constant δt is thus imposed (cf. Table 1).

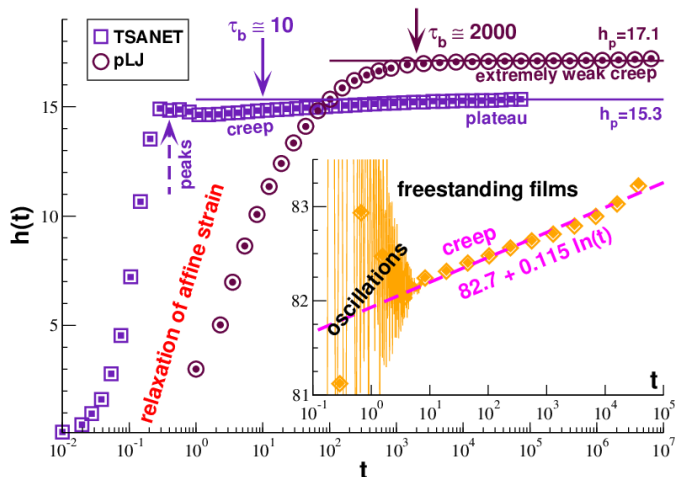


Fig. 2. Shear-stress correlation function h (open symbols) and (rescaled) standard deviation $\delta h/\sqrt{2}$ (filled symbols) as functions of time t . The vertical arrows mark the approximate position of τ_b where $h(t)$ becomes constant. $\delta h(t)/\sqrt{2} \approx h(t)$ holds to high accuracy confirming the Gaussianity of the stochastic process. Inset: Strong short-time oscillations followed by a weak logarithmic creep behavior for polymer films.

and δv_{ext} become rapidly n_k -independent for $n_k \gg 1$. Due to the imposed Δt_{max} the latter method is limited to $\Delta t \leq \Delta t_{\text{max}}/n_k$ and the spacer time interval Δt_{spac} (marked by open circles in Fig. 1) between the sampling time interval Δt (filled circles) is not constant but decreases with n_k and Δt and vanishes for $\Delta t = \Delta t_{\text{max}}/n_k$. Fortunately, the latter point is irrelevant for the non-ergodic systems with $\tau_\alpha \gg \Delta t_{\text{max}} \gg \Delta t + \Delta t_{\text{spac}} \gg \tau_b$, i.e. subsequent time series are decorrelated and $n_k \gg 1$. It may matter, however, for the analysis of temperature effects as briefly discussed in Sec. 4.6.

4 Shear-stress fluctuations

4.1 Autocorrelation function $h(t)$

We turn now to the presentation of our numerical results on the shear-stress fluctuations of the three model systems. As shown in Fig. 2 we begin with the ACF $h(t)$. We remind that within linear response $h(t)$ is equivalent (apart an additive constant μ_A and a minus sign) to the shear-stress relaxation function $G(t) = \mu_A - h(t)$ [21,27,14,15] commonly measured in experimental studies [8,9]. Let us focus first on the data for pLJ particles (circles) obtained by means of local MC moves of the beads and presented in the main panel. (Time is given for this model in units of MC attempts for all n particles.) Trivially, $h(0) = 0$. $h(t)$ first increases rapidly for $t \ll \tau_b$, corresponding physically to the relaxation of an affine shear strain imposed at $t = 0$ [21,27], and becomes then essentially constant, $h(t) \rightarrow h_p = 17.1$, for more than three orders of magnitude as emphasized by the upper horizontal line. To estimate the basin relaxation time $\tau_b \approx 2000$ quantitatively we have used the criterion

$h(t \approx \tau_b) = f h_p$ setting (slightly arbitrarily) $f = 0.99$. Note that $h(t)$ is strictly monotonically increasing (no oscillations) and that a zoom of the plateau regime reveals (not visible) an extremely weak logarithmic creep with $h(t) \approx 16.98 + 0.01 \ln(t)$ for $t \gg \tau_b$.

The behavior observed for our models using MD simulations (TSANET, polymer films) is unfortunately more complex revealing both non-monotonic behavior (at short times) and much stronger logarithmic creep. As may be seen from the main panel, the overdamped TSANET model shows after a maximum at $t \approx 0.3$ (being in fact two peaks superimposed and merged in this representation due to the logarithmic horizontal time scale) a minimum at $t \approx 1$ followed by a weak logarithmic creep with $h(t) \approx 14.5 + 0.1 \ln(t)$ up $t \approx 10^4$ and then eventually a constant plateau with $h_p = 15.3$ (middle horizontal line). (Using $\Delta t_{\text{max}} = 10^7$ and $\delta t = 1$ we have verified that this is indeed the terminal plateau value for these quenched elastic networks.) What is the relaxation time τ_b for the metabasins of the quenched TSANET model? One reasonable value is $\tau_b \approx 10^4$ characterizing the time where $h(t)$ becomes rigorously constant, another $\tau_b \approx 10^3$ if we insist on the above criterion with $f = 0.99$. These two values appear, however, far too conservative for many properties discussed below being integrals over $h(t)$ for which $\tau_b \approx 10$ (vertical arrow) is a more realistic estimate.

The inset presents $h(t)$ for polymer films focusing on the data around $h(t) \approx 82$. Strong oscillations are seen for short times $t \ll 10$. The effect is much stronger than for the TSANET model due to the strong bonding potential [20] along the polymer chains and the Nosé-Hoover thermostat used for these MD simulations. (A strong Langevin thermostat was used for the TSANET model.) As already pointed out in Ref. [15], a logarithmic creep with $h(t) \approx 82.7 + 0.12 \ln(t)$ is observed for $t \gg 10$. The logarithmic creep coefficient is similar to the one observed at intermediate times for the TSANET model but no final plateau is observed. The thin polymer films are thus not rigorously non-ergodic, just as the pLJ model.¹¹ Fortunately, the logarithmic creep coefficients are rather small for all models. On the logarithmic scales (power-law behavior) we focus on below this effect will be seen to be less crucial merely causing higher order corrections with respect to the idealized behavior sketched in Sec. 2.

Also indicated in Fig. 2 are the rescaled standard deviations $\delta h/\sqrt{2}$ (filled symbols). As explained in Sec. III.1 of Ref. [15], these were computed using gliding averages along the trajectories as the last step. We remind that if instantaneous shear stresses correspond to a stationary Gaussian process, this implies [15]

$$\delta h(t)^2 = 2h(t)^2. \quad (54)$$

¹¹ Only the TSANET systems for $\nu = 0$ are rigorously non-ergodic for $\Delta t_{\text{max}} \rightarrow \infty$. The film system is in a transient regime with a wide spectrum of relaxation times both below and above Δt_{max} . As a result Eq. (35) cannot hold exactly. As for the pLJ model, its relaxation time spectrum is apparently well below Δt_{max} .

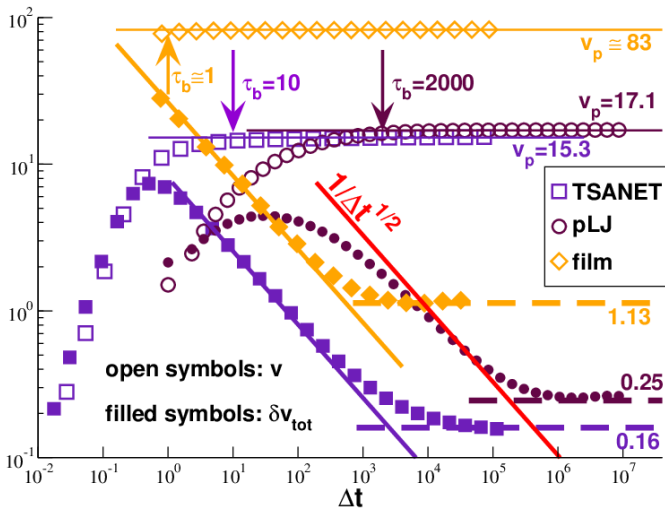


Fig. 3. Shear-stress fluctuation v and the corresponding total standard deviation δv_{tot} (filled symbols) as functions of the sampling time Δt . The thin horizontal solid lines mark the long-time plateau value v_p , the vertical arrows the relaxation time τ_b of the different models. While $\delta v_{\text{tot}} \propto 1/\sqrt{\Delta t}$ for intermediate times (bold solid lines), a leveling-off $\delta v_{\text{tot}} \rightarrow \Delta_{\text{ne}}$ is observed for large times (bold dashed horizontal lines) with $\Delta_{\text{ne}} = 0.16$ for TSANET, $\Delta_{\text{ne}} = 0.25$ for the pLJ particles and $\Delta_{\text{ne}} = 1.13$ for the freestanding polymer films.

As can be seen, Eq. (54) holds nicely for all our models. A more precise characterization of the Gaussianity of the stochastic process is obtained using the non-Gaussianity parameter $\alpha_2 = \delta h^2 / 2h(t)^2 - 1$ [7]. For our standard system sizes this yields very tiny values, e.g., $\alpha_2 \approx 0.0002$ for pLJ particles.¹²

4.2 Variance v and standard deviation δv_{tot}

Using a double-logarithmic representation we compare in Fig. 3 the shear-stress fluctuation v with the corresponding total standard deviation δv_{tot} (filled symbols). We remind that $v(\Delta t)$ is connected with $h(t)$ via Eq. (4). Being a second integral over $h(t)$, $v(\Delta t)$ is a much smoother and numerically better behaved property [15]. Due to this v increases monotonically without oscillations and non-monotonic behavior for all three models. Moreover, since the vertical axis is logarithmic the weak creep of the data mentioned in Sec. 4.1 becomes irrelevant, i.e. essentially $v(\Delta t) \rightarrow v_p = \text{const}$ for $\Delta t \gg \tau_b$ as emphasized for all models by the thin horizontal lines marking the plateau value v_p and the vertical arrows for the basin relaxation time τ_b . (As implied by Eq. (4) $v_p \approx h_p$ for all models.) This allows to define τ_b using the *same* criterion for all models by setting

$$v(\Delta t \stackrel{!}{=} \tau_b) = f v_p \text{ with } f = 0.95 \quad (55)$$

¹² The non-Gaussianity parameter α_2 is seen to increase somewhat for smaller system sizes. The typical values are, however, always rather small, e.g., $\alpha_2 \ll 0.04$ for all times for pLJ particles with $n = 100$.

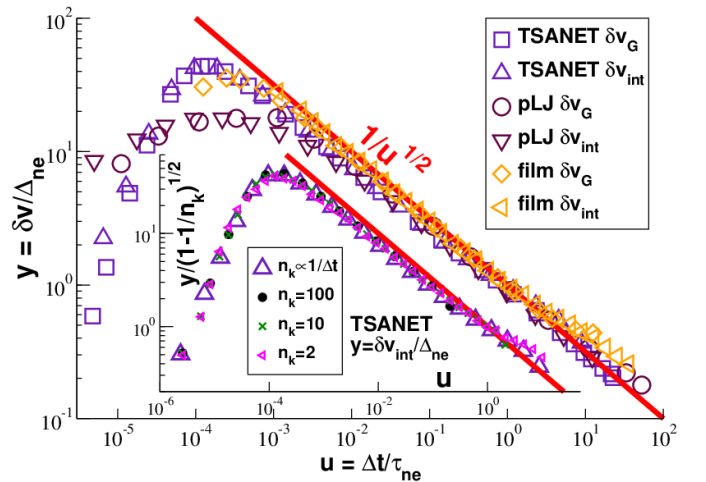


Fig. 4. Main panel: Comparison of δv_G and δv_{int} using a double-logarithmic representation. The reduced standard deviations $y = \delta v / \Delta_{\text{ne}}$ are plotted as functions of the reduced sampling time $u = \Delta t / \tau_{\text{ne}}$ with $\tau_{\text{ne}} = 4200$ for the TSANET model, $\tau_{\text{ne}} = 200000$ for the pLJ particles and $\tau_{\text{ne}} = 800$ for the polymer films. The bold solid line marks the expected power-law decay $y \approx 1/\sqrt{u}$. Inset: $y = \delta v_{\text{int}}(\Delta t, n_k) / \Delta_{\text{ne}}$ rescaled as $y / (1 - 1/n_k)^{1/2}$ vs. u for the TSANET model and different n_k . The perfect data collapse for $n_k \geq 2$ is expected from Eq. (46).

being chosen to obtain the same $\tau_b \approx 2000$ for the pLJ particles as in Sec. 4.1. This gives the values stated in Table 1. (See Fig. 9 below for the system-size dependence of τ_b for pLJ particles.)

The total standard deviation δv_{tot} , computed by averaging over all available time series \mathbf{x}_{ck} , Eq. (18), has a maximum about a decade below τ_b . This is expected from the strong increase of $h(t)$ and $v(\Delta t)$ in this time window [15]. As emphasized by the bold solid lines, $\delta v_{\text{tot}}(\Delta t)$ decreases then following roughly the $1/\sqrt{\Delta t}$ -decay expected for $\tau_b \ll \Delta t \ll \tau_{\text{ne}}$. δv_{tot} becomes constant, $\delta v_{\text{tot}} \rightarrow \Delta_{\text{ne}}$, for large Δt for all models (bold dashed horizontal lines). As explained in Sec. 2.2, this is a generic behavior expected for non-ergodic systems. We determine the values $\Delta_{\text{ne}} = 0.16$ for TSANET, $\Delta_{\text{ne}} = 0.25$ for the pLJ particles and $\Delta_{\text{ne}} = 1.13$ for the freestanding polymer films. These values are used in the next subsection to rescale the standard deviations δv .

4.3 Comparison of δv_G and δv_{int}

We compare δv_G and δv_{int} in the main panel of Fig. 4. $\delta v_G[h]$ has been determined by means of a numerical more suitable reformulation of Eq. (5) described in Refs. [14, 15] using the ACF $h(t)$ shown in Fig. 2. δv_{int} was obtained according to Eq. (19) using $n_k \propto 1/\Delta t$ time series k as described in Sec. 3.3. Most importantly, $\delta v_G \approx \delta v_{\text{int}}$ appears to hold for all Δt confirming thus Eq. (45) and the assumption that the trajectories within each meta-basin are stationary Gaussian processes. Moreover, plotting the reduced standard deviations $y = \delta v / \Delta_{\text{ne}}$ of the three models as functions of the reduced sampling time $u = \Delta t / \tau_{\text{ne}}$

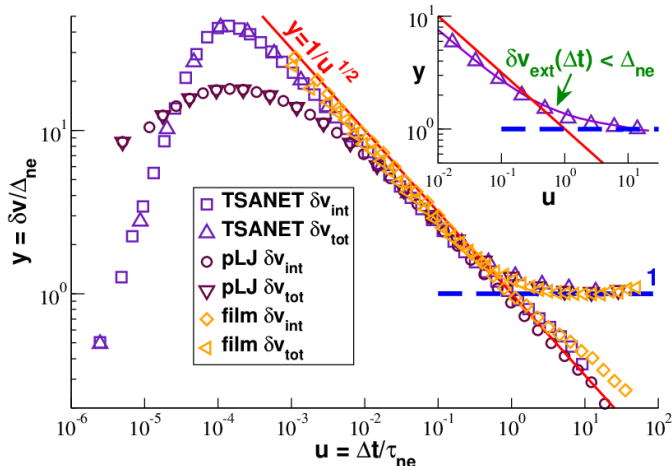


Fig. 5. Main panel: Comparison of δv_{int} and δv_{tot} using double-logarithmic coordinates with $y = \delta v / \Delta_{\text{ne}}$ and $u = \Delta t / \tau_{\text{ne}}$. $\delta v_{\text{int}} \approx \delta v_{\text{tot}}$ holds for $u \ll 1$ while $\delta v_{\text{tot}} \rightarrow 1$ for $u \gg 1$ (bold dashed line). Inset: $y = \delta v_{\text{tot}}(\Delta t) / \Delta_{\text{ne}}$ vs. u . As shown for the TSANET model, Eq. (47) gives a good approximation for δv_{tot} . Tiny deviations are seen for $u \approx 1$.

leads to a data collapse for all three models for $u \gg \tau_{\text{b}} / \tau_{\text{ne}}$. Importantly, all data essentially decay as $y \approx 1/\sqrt{u}$ (bold solid line) in the scaling regime. Note that a free power-law fit would yield a slightly weaker exponent for all models. This small deviation may be attributed to the fact that the ACFs $h(t)$ of none of the models is exactly constant, $h(t) = h_{\text{p}}$, as shown in Sec. 4.1 at variance to Eq. (35). As already pointed out in Ref. [15], deviations are especially seen for polymer films for $u \gg 1$.

The inset of Fig. 4 presents in more detail $y(u) = \delta v_{\text{int}} / \Delta_{\text{ne}}$ for the TSANET model comparing data obtained for different numbers n_{k} of time series k for each configuration c . The large triangles represent the same data shown in the main panel where $n_{\text{k}} \propto 1/\Delta t$, all other data have been obtained with a fixed number n_{k} as indicated. We remind that $\delta v_{\text{int}} = 0$ for $n_{\text{k}} = 1$. A direct plot of y (not shown) reveals that all data but those for $n_{\text{k}} \leq 10$ collapse, i.e. the n_{k} -dependence becomes rapidly irrelevant. An even better data collapse for all data with $n_{\text{k}} \geq 2$ is obtained as suggested by Eq. (46) using the rescaled standard deviation $y/(1 - 1/n_{\text{k}})^{1/2}$. In other words it is sufficient to use $n_{\text{k}} = 2$ time series for one configuration to obtain using the rescaling factor $(1 - 1/n_{\text{k}})^{1/2}$ the asymptotic limit. This finding should strongly simplify future numerical work.

4.4 Comparison of δv_{int} and δv_{tot}

We compare δv_{tot} with δv_{int} in Fig. 5 using reduced units with $y = \delta v / \Delta_{\text{ne}}$ and $u = \Delta t / \tau_{\text{ne}}$. We remind that τ_{ne} (Tab. 1) has been determined as a crossover time by means of Eq. (38) using the measured Δ_{ne} and $\delta v_{\text{int}}(\Delta t)$. Apart very short (reduced) sampling times u , the rescaled data depend very little on the model on the logarithmic scales considered. As expected, $\delta v_{\text{tot}} \approx \delta v_{\text{int}}$ holds to high precision for all $u \ll 1$. All data sets decrease essentially

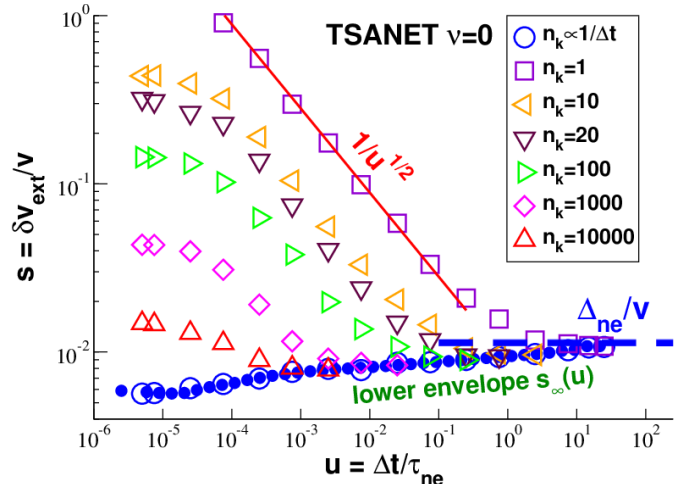


Fig. 6. $s = \delta v_{\text{ext}} / v$ vs. $u = \Delta t / \tau_{\text{ne}}$ for quenched TSANET networks. The large open and small filled circles have been obtained using $n_{\text{k}} \propto 1/\Delta t$, all other symbols by imposing a constant n_{k} . The thin solid line indicates the expected power-law behavior $s \approx 1/\sqrt{u}$ for small n_{k} , the bold dashed horizontal line the asymptotic limit $s \rightarrow \Delta_{\text{ne}} / v$ for $u \gg 1$.

as $y \approx 1/\sqrt{u}$ for $u \gg u_{\text{b}}$ over nearly three orders of magnitude as emphasized by the bold solid line. While the $1/\sqrt{u}$ -decay continues for δv_{int} for large $u \gg 1$, the rescaled δv_{tot} -data levels off to the plateau indicated by the horizontal dashed line.

Focusing on the TSANET model we test the interpolation formula Eq. (47) in the inset of Fig. 5, i.e. we compare the directly measured δv_{tot} (triangles) with $(\delta v_{\text{int}}^2(\Delta t) + \Delta_{\text{ne}}^2)^{1/2}$ (solid line).¹³ The same result is obtained by replacing δv_{int} by δv_{G} as expected from Fig. 4 (not shown). The interpolation formula is seen to give an excellent fit of δv_{tot} . To leading order δv_{tot} is thus given by $\delta v_{\text{int}} \approx \delta v_{\text{G}}$ and, hence, by $h(t)$ plus an additional constant. As indicated by the arrow, Eq. (47) slightly *overpredicts* δv_{tot} for $u \approx 1$. Apparently, $\delta v_{\text{ext}}(u)$ approaches its asymptotic limit Δ_{ne} from below.

4.5 Characterization of $\delta v_{\text{ext}}(\Delta t, n_{\text{k}})$

This point is further investigated in Fig. 6 presenting the dimensionless standard deviation $s = \delta v_{\text{ext}}(\Delta t, n_{\text{k}}) / v(\Delta t)$ for the TSANET model. (See Fig. 8 for the unscaled δv_{ext} -data for pLJ particles.) As emphasized in Sec. 2.2, δv_{ext} depends in general on Δt and may also depend on n_{k} . The data indicated by the large open and the small filled circles have been both obtained for $n_{\text{k}} \propto 1/\Delta t$ as described in Sec. 3.3. To demonstrate the *numerical* equivalence of both definitions the small filled circles are computed using $\delta v_{\text{ext}}^2 = \delta v_{\text{tot}}^2 - \delta v_{\text{int}}^2$, Eq. (6), and the large circles using directly Eq. (20).

¹³ Eq. (47) is applicable for $\Delta t \gg \tau_{\text{b}}$. In terms of u this condition becomes $u \gg 1/400$ for the TSANET model. This is roughly satisfied by the u -range presented in Fig. 5.

It is also instructive to characterize s for different fixed numbers n_k of equidistant and non-overlapping time series decoupling thus Δt and n_k . We remind that $\delta v_{\text{ext}} = \delta v_{\text{tot}}$ for $n_k = 1$ and the power-law slope indicated for the intermediate Δt -regime of this data set corresponds to the $1/\sqrt{\Delta t}$ -decay already shown in Fig. 5. Confirming Sec. 2.2, s becomes n_k -independent for large n_k approaching a lower envelope $s_\infty(\Delta t) = \lim_{n_k \rightarrow \infty} s(\Delta t, n_k)$ from above. This lower envelope corresponds essentially to the circles. $s_\infty(\Delta t)$ is seen to *increase monotonically*, albeit extremely weakly, approaching Δ_{ne}/v (dashed line) from below. This is consistent with the tiny deviations from δv_{tot} observed for the shifted δv_{int} -data in the inset of Fig. 5. Similar results have been obtained for the other models as seen in the inset of Fig. 7 showing $\delta v_{\text{ext}}(\Delta t, n_k)$ for the pLJ particles.

We note finally that Eq. (39) implies in principle that

$$n_k (\delta v_{\text{ext}}^2(\Delta t, n_k) - \Delta_{\text{ne}}^2) \simeq \delta v_{\text{int}}^2(\Delta t) \geq 0 \quad (56)$$

for $\Delta t \gg \tau_b$. This allows to express $\delta v_{\text{ext}}(\Delta t, n_k)$ in terms of $\delta v_{\text{int}}(\Delta t) \approx \delta v_G[h]$ for small Δt and n_k (not shown). Unfortunately, this is not possible in the opposite limit since $\delta v_{\text{ext}}^2(\Delta t, n_k) - \Delta_{\text{ne}}^2$ becomes negative as seen by the monotonic increase of $s_\infty(\Delta t)$. It is better to go back to the more general Eq. (32) which can be rephrased as

$$\delta v_{\text{ext}}(\Delta t) \simeq (\delta v_{\text{ext}}^2(\Delta t, n_k) - \delta v_G^2[h]/n_k)^{1/2}. \quad (57)$$

As shown in the inset of Fig. 7 by the large crosses for $n_k = 10$ this may be used to obtain the asymptotic $\delta v_{\text{ext}}(\Delta t)$ from $\delta v_{\text{ext}}(\Delta t, n_k)$ and $\delta v_G[h]$, at least if $\delta v_G[h]$ is available with sufficient precision.

4.6 Temperature dependence of δv_{ext}

A different representation of δv_{ext} is chosen in the main panel of Fig. 7 where data sets for fixed sampling times Δt (increasing from bottom to top) are plotted as functions of n_k . Extending beyond the main focus of this work on non-ergodic systems we compare here data sets for a broad range of temperatures T . The dimensionless vertical axis $y = \delta v_{\text{ext}}(n_k)/\delta v_{\text{ext}}(n_k = 1)$ is used to normalize all data sets for different Δt and T and to compare δv_{ext} with $\delta v_{\text{tot}} = \delta v_{\text{ext}}(n_k = 1)$. $y \ll 1$ implies that $\delta v_{\text{tot}} \approx \delta v_{\text{int}}$, i.e. both averaging procedures become equivalent. The bold solid line indicates the power law $1/\sqrt{n_k}$ expected for independent time series \mathbf{x}_{ck} being a *lower envelope for all data sets*. This envelope is the more relevant the smaller Δt and the higher T . This is especially the case for all high temperatures where the systems are ergodic and according to Eq. (41) we have

$$\delta v_{\text{ext}}(\Delta t, n_k) \simeq \frac{\delta v_{\text{int}}(\Delta t)}{\sqrt{n_k}} = \frac{\delta v_G[h]}{\sqrt{n_k}} \quad (58)$$

for $n_c \rightarrow \infty$. In agreement with Fig. 6 and the inset of Fig. 7, δv_{ext} increases with Δt and becomes n_k -independent for large Δt and low T . Note that the n_k -dependence is weak for $\Delta t = 10^6$ and $T = 0.2$ and $T = 0.19$.

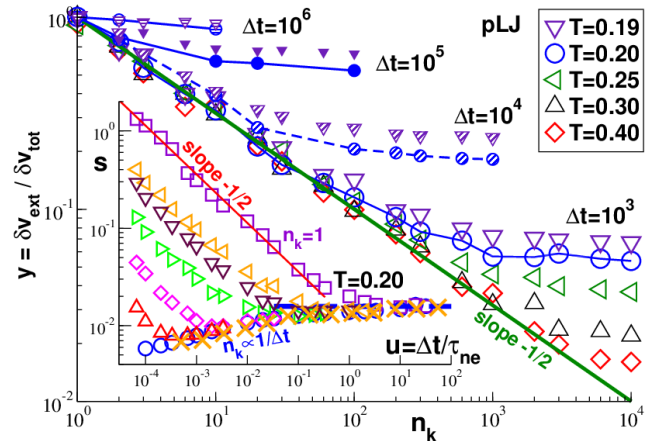


Fig. 7. $\delta v_{\text{ext}}(\Delta t, n_k)$ for pLJ particles. Inset: $s = \delta v_{\text{ext}}/v$ vs. Δt for $T = 0.2$ for different n_k using the same symbols as in Fig. 6. The thin solid line indicates the power-law slope $-1/2$ for $\delta v_{\text{ext}}(n_k = 1) = \delta v_{\text{tot}}$, the solid dashed line the large- Δt limit Δ_{ne}/v . With increasing n_k all data sets approach a lower n_k -independent envelope $s_\infty(\Delta t)$. A good estimation of this limit is given by the data for $n_k \propto 1/\Delta t$ (circles). The crosses represent the rescaled $\delta v_{\text{ext}}(\Delta t, n_k)$ for $n_k = 10$ using $\delta v_G[h]$ and the approximation Eq. (57). Main panel: $y = \delta v_{\text{ext}}/\delta v_{\text{tot}}$ vs. n_k for $\Delta t = 10^3, 10^4, 10^5$ and 10^6 (from bottom to top) for several temperatures. Open symbols are used for $\Delta t = 10^3$, filled symbols for $\Delta t = 10^5$. The data for $T = 0.2$ is connected by lines. The bold solid line indicates the power-law $-1/2$ expected for independent time series.

A technical issue relevant for future work should be mentioned here. Closer inspection of the data for $T = 0.3$ and $T = 0.4$ shows in fact a small upbending for the largest n_k which is not consistent with Eq. (58). We remind that we have stored for each configuration c only one trajectory of constant length Δt_{max} , i.e. the spacer interval Δt_{spac} between the used time series of length $\Delta t \leq \Delta t_{\text{max}}/n_k$ decreases strongly with Δt and n_k . Neighboring Δt -intervals become thus correlated once Δt_{spac} gets smaller than the terminal relaxation time $\tau_\alpha(T)$ [7,9]. One simple means to test that the observed upbending at high temperatures is merely due to this technical effect would be to increase Δt_{max} and thus Δt_{spac} by, say, a factor 10 or 100. The upbending must then be shifted to correspondingly larger Δt . Larger Δt_{max} are in any case warranted to better show for $T \ll T_g$ that $\delta v_{\text{ext}}(\Delta t) \rightarrow \Delta_{\text{ne}}$ for large Δt . However, for a physical meaningful characterization of δv_{ext} for intermediate temperatures it would be even better to work with a *constant* spacer time Δt_{spac} for all temperatures and to sample thus n_k sequences of fixed spacer and measurement time intervals decoupling thus n_k from both Δt and Δt_{spac} . $y \approx 1/\sqrt{n_k}$ must then rigorously hold for $\Delta t_{\text{spac}} \gg \tau_\alpha$ while y should reveal a (possibly temperature dependent) shoulder in the opposite limit. The next challenge to be addressed then is of whether a time-temperature superposition scaling using the directly measured terminal relaxation $\tau_\alpha(T)$ is possible or not.

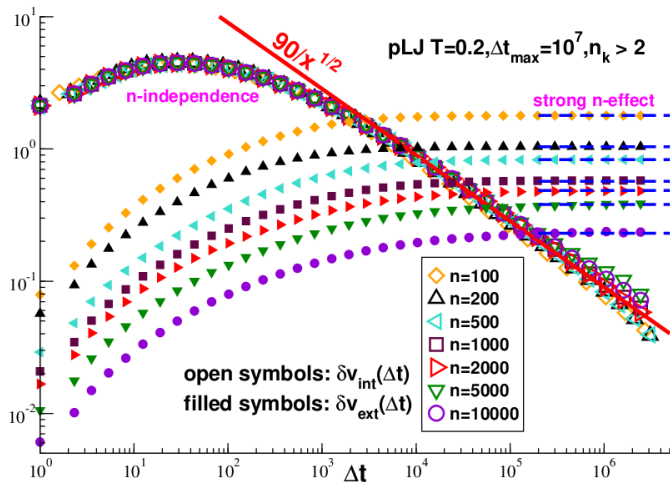


Fig. 8. δv_{int} (open symbols) and δv_{ext} for pLJ systems for a broad range of particle numbers n . δv_{int} is essentially n -independent, i.e. $\gamma_{\text{int}} = 0$, while δv_{ext} decreases with n . The bold solid line indicates the decay of δv_{int} expected according to Eq. (35), the dashed horizontal lines show the δv_{ext} -values given in Fig. 9.

4.7 System-size dependence

We investigate now the dependence of several properties on the system size focusing on data obtained for the pLJ particles. We have seen above that the total variance δv_{tot}^2 of the shear-stress fluctuations v of quenched elastic bodies may be decomposed as the sum of two contributions due to independent physical causes: the internal and external variances δv_{int}^2 and δv_{ext}^2 . The main point made in this subsection is that δv_{int} and δv_{ext} are characterized by different n -dependences. Figure 8 compares the Δt -dependences of δv_{int} and δv_{ext} for different particle numbers n . δv_{int} and δv_{ext} have been computed using $n_k \propto 1/\Delta t$ time series for each configuration. The data are plotted as functions of the unscaled sampling time Δt in units of MC steps. The bold solid line indicates the decay of δv_{int} expected according to Eq. (35) for $\Delta t \gg \tau_b$. As can be seen, δv_{int} is essentially n -independent, i.e. $\gamma_{\text{int}} = 0$ as expected if standard statistical physics holds for each meta-basin. At striking variance to this δv_{ext} strongly decreases with n , i.e. the v_c become similar, and becomes constant, $\delta v_{\text{ext}} \rightarrow \Delta_{\text{ne}}$, for large Δt . Interestingly, $\delta v_{\text{int}}(\Delta t)$ is a monotonically decreasing function of Δt while $\delta v_{\text{ext}}(\Delta t)$ is always monotonically increasing. Note that the increase of $\delta v_{\text{ext}}(\Delta t)$ for $\Delta t \ll \tau_b$ is much stronger than the one seen for the reduced external standard deviation $s_\infty(\Delta t)$ in Fig. 6 and the inset of Fig. 7. In other words, the Δt -dependence of $\delta v_{\text{ext}}(\Delta t)$ stems mainly from the Δt -dependence of $v(\Delta t)$, Fig. 3.

The n -dependence of various properties is presented in Fig. 9. We compare in the main panel h , v , δv_G , δv_{int} , δv_{ext} and δv_{tot} measured at $\Delta t = 10^6$ with the non-ergodicity parameter Δ_{ne} (circles). As emphasized by the dashed horizontal lines, h , v and $\delta v_G \approx \delta v_{\text{int}}$ are all independent of the particle number n , i.e. $\gamma_{\text{int}} = 0$ as expected from Sec. 2.5. Moreover, δv_{ext} , δv_{tot} and Δ_{ne} are

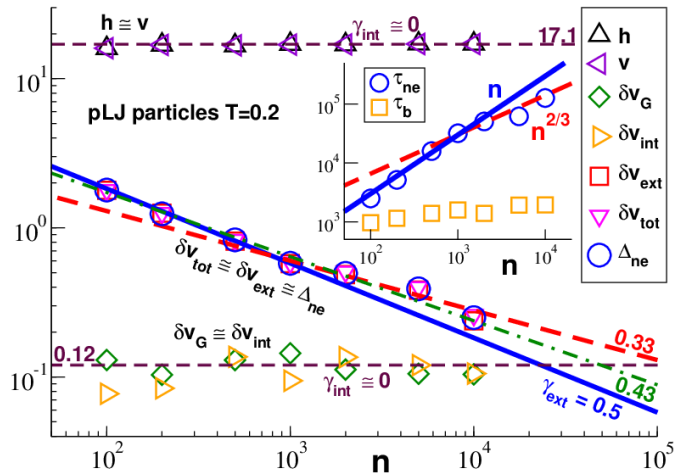


Fig. 9. Dependence on particle number n for various properties for pLJ particles. Main panel: h , v , δv_G , δv_{int} , δv_{tot} for $\Delta t = 10^6$ and Δ_{ne} . The thin horizontal dashed lines indicate the exponent $\gamma_{\text{int}} = 0$, the bold solid line $\gamma_{\text{ext}} = 1/2$, the dash-dotted line $\gamma_{\text{ext}} \approx 0.43$ and the bold dashed line $\gamma_{\text{ext}} \approx 0.33$. Inset: n dependence of τ_b and τ_{ne} . While τ_b saturates for large n , τ_{ne} increases with n broadly in agreement with Eq. (50).

within numerical accuracy identical. This is expected since $\Delta t = 10^6 \gg \tau_{\text{ne}}$ for all n . Δ_{ne} was seen to decrease with a power-law exponent $\gamma_{\text{ext}} = 1/2$ for the TSANET model [15]. According to Eq. (49) this suggests that independent localized shear-stress fluctuations are relevant for these elastic networks. Interestingly, a weaker exponent $\gamma_{\text{ext}} \approx 1/3$ (bold solid line) has been fitted in recent simulation studies of 2D binary LJ mixtures [16], dense 3D polymer glasses [14] and to the 2D pLJ particles [15] also investigated in the present study. A somewhat larger exponent $\gamma_{\text{ext}} \approx 0.43$ (dash-dotted line) appears to better fit all currently available pLJ data. Assuming that future simulations confirm that $\gamma_{\text{ext}} < 1/2$ this could be explained by long-range spatial correlations with a *diverging* correlation length ξ [28, 14, 30].

As can be seen from the inset, the basin relaxation time τ_b , obtained using Eq. (55) from $v(\Delta t)$, only depends weakly (logarithmically) on n . At variance to this $\tau_{\text{ne}}(n)$, obtained using Eq. (38), strongly increases. The two indicated power-law slopes are attempts to characterize this dependence. According to Eq. (50) one expects $\tau_{\text{ne}} \propto n^{2\gamma_{\text{ext}}}$ for $\gamma_{\text{int}} \approx 0$. Depending on whether $\gamma_{\text{ext}} = 1/2$ or $\gamma_{\text{ext}} \approx 1/3$, this corresponds either to $\tau_{\text{ne}} \propto n$ (bold solid line) or $\tau_{\text{ne}} \propto n^{2/3}$ (dashed line). The linear relation only fails for the two largest systems.

5 Conclusion

Extending our recent work focusing on ergodic stationary Gaussian stochastic processes [14, 15] on to non-ergodic systems, we have described in general terms the standard deviation $\delta v(\Delta t)$ of the empirical variance $v[\mathbf{x}]$, Eq. (3), of time series \mathbf{x} measured over a finite sampling time Δt . Since independent “configurations” c get trapped in meta-

basins of the generalized phase space (Fig. 1) it becomes relevant in which order c -averages and c -variances over configurations c and k -averages and k -variances over time series k of a given configuration c (Sec. 2.1) are performed. Three types of variances of $v[\mathbf{x}_{ck}]$ must be distinguished: the total variance δv_{tot}^2 , Eq. (18), the internal variance δv_{int}^2 within each meta-basin, Eq. (19), and the external variance δv_{ext}^2 between the different basins, Eq. (20). It was shown (Sec. 2.2) that $\delta v_{\text{tot}}^2 = \delta v_{\text{int}}^2 + \delta v_{\text{ext}}^2$, Eq. (6). Various general and more specific simplifications of our key relation Eq. (6) are given for physical systems where the stochastic process $x(t)$ is due to a fluctuating density field averaged over the system volume V . Assuming the stochastic process within each basin to be thus (essentially) Gaussian, δv_{int} is given by the functional $\delta v_{\text{G}}[h]$, Eq. (5), in terms of the c -averaged ACF h , Eq. (45). Both the Δt - and the V -dependence of δv_{int} is thus imposed by $h(t)$. Specifically, this implies that $\delta v_{\text{int}}(\Delta t) \approx \delta v_{\text{G}}(\Delta t) \propto 1/\sqrt{\Delta t}$ for $\Delta t \gg \tau_b$. Moreover, δv_{ext} converges for $\Delta t \gg \tau_b$ to the constant “non-ergodicity parameter” Δ_{ne} . Since $\delta v_{\text{ext}} \approx \Delta_{\text{ne}}$ decreases more strongly with the system volume V than δv_{int} (Sec. 2.5), the non-ergodicity time $\tau_{\text{ne}}(V)$, Eq. (38), must increase with V . Deviations of δv_{tot} from $\delta v_{\text{int}} \approx \delta v_{\text{G}}$ are thus merely finite-size effects.

We have illustrated and essentially confirmed these relations in Sec. 4 for stochastic processes obtained from the (reduced) shear stresses $x(t) = \sqrt{\beta V} \hat{\sigma}(t)$ computed in amorphous solids. Quenched elastic networks and two low-temperature glasses have been compared. The Gaussianity approximation $\delta v_{\text{int}} \approx \delta v_{\text{G}}[h]$, Eq. (45), is seen to hold for all Δt (Fig. 4), i.e. $\delta v_{\text{int}}(\Delta t)$ is set by $h(t)$. Interestingly, δv_{ext} is seen to approach its asymptotic limit $\delta v_{\text{ext}} \approx \Delta_{\text{ne}}$ from below (Figs. 6, 7 and 8). The discussion in Secs. 4.3-4.5 has focused on the comparison of δv_{int} , δv_{G} , δv_{tot} and δv_{ext} for one state point, i.e. one temperature and one system size. Effects of the volume $V \propto n$ have been considered in Sec. 4.7. While h , v , $\delta v_{\text{G}} \approx \delta v_{\text{int}}$ are essentially V -independent ($\gamma_{\text{int}} \approx 0$) as expected for stochastic processes of intensive thermodynamic fields (Sec. 2.5), $\delta v_{\text{ext}} \approx \Delta_{\text{ne}} \propto 1/V^{\gamma_{\text{ext}}}$ strongly decreases (Fig. 9). That δv_{int} and δv_{ext} are independent contributions to δv_{tot} characterized by different statistics is thus manifested by their different V -dependences. While an exponent $\gamma_{\text{ext}} = 1/2$ has been fitted for the TSANET model [15], a weaker (apparent) exponent $\gamma_{\text{ext}} < 1/2$ appears to fit Δ_{ne} for the pLJ particles. As already pointed out elsewhere [14] this suggests long-range spatial correlations.

Temperature effects have been mentioned briefly for pLJ particles and the external variance δv_{ext}^2 (Sec. 4.6). As pointed out there, future studies should increase the total sampling times Δt_{max} for each configuration to better describe the scaling of δv_{int} and δv_{ext} with Δt and n_k for different temperatures. Especially, it should be useful to sample these properties using a fixed spacer time interval Δt_{spac} for all temperatures. While $\delta v_{\text{ext}}(n_k) \propto 1/\sqrt{n_k}$ for high temperatures (Fig. 7), $\delta v_{\text{ext}}(n_k)$ should reveal an intermediate plateau (shoulder), Δ_{ne} , before it decays for even larger n_k . A central question is then whether this intermediate plateau $\Delta_{\text{ne}}(T)$ depends continuously on T

— as suggested by our data (Fig. 7) — or if a jump-singularity appears [30].

We have considered in the present work the standard deviations δv associated with the empirical variance $v[\mathbf{x}]$, Eq. (3), with $p = 2$. It is straightforward to generalize our approach to other moments p . Especially, Eq. (6) still holds and the generalized internal variance δv_{int}^2 must be given by a generalization of $\delta v_{\text{G}}^2[h]$, i.e. one expects the same V -dependence for h and $\delta v_{\text{int}} \approx \delta v_{\text{G}}$. Probing different moments p should make manifest the higher-order spatial correlations of the instantaneous stress field $\hat{\sigma}_r$. Note that the expectation values v for $p = 2, 3, \dots$ correspond to important contributions to the generalized stress-fluctuation formalism for the p -order elastic moduli B_p (being the p -order strain derivative of the free energy) [15,16]. Surprisingly, the standard deviations δB_p for $p > 2$ have been claimed to diverge with increasing V leading to a “breakdown of nonlinear elasticity in amorphous solids” [16]. Since the common every day experience is rather that sufficiently large amorphous (plastic) bodies are well behaved according to standard continuum mechanics [8,9,10], the presented work suggests that the experimentally relevant standard deviations should be characterized by internal standard deviations $\delta B_{p,\text{int}}$ using Eq. (19) instead of the total standard deviations $\delta B_{p,\text{tot}}$ computed using Eq. (18) in Ref. [16]. We are currently working out the consequences of this idea.¹⁴

Author contribution statement

JB and JPW designed the research project. The presented theory was gathered from different sources by ANS and JPW. GG (polymer films), LK (pLJ particles) and JPW (TSANET) performed the simulations and the data analysis. JPW wrote the manuscript benefiting from contributions of all authors.

Acknowledgments

We are indebted to O. Benzerara for helpful discussions and acknowledge computational resources from the HPC cluster of the University of Strasbourg.

A System-size exponents γ_{int} and γ_{ext}

We focus here on properties obtained for $\Delta t \gg \tau_b$. The time dependence becomes thus irrelevant. Due to the non-ergodicity the c -dependence remains relevant, however,

¹⁴ The stress-fluctuation formalism for B_p uses the fluctuations of stationary stochastic processes, i.e. no external (linear) perturbation is applied to measure directly the moduli. It is unclear whether the out-of-equilibrium processes are described by the same fluctuations. It is an open theoretical question of how to generalize the fluctuation-dissipation relations, connecting the *average* linear out-of-equilibrium response to the *average* equilibrium relaxation [5,7,17], for their fluctuations.

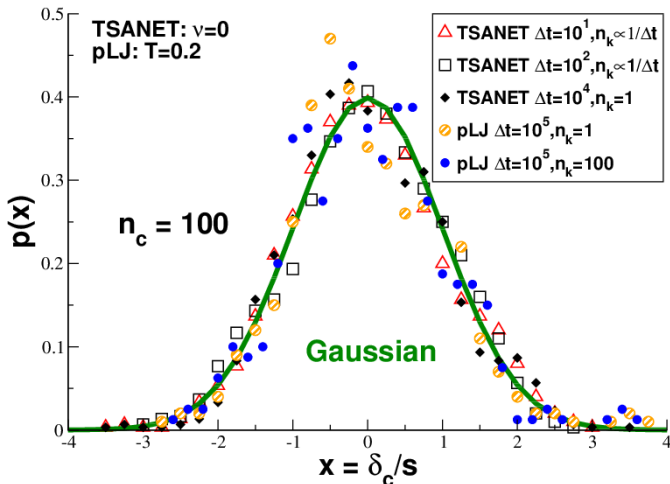


Fig. 10. Normalized histogram $p(x)$ for different Δt and n_k as indicated. The histograms are well described by a Gaussian (bold solid line).

and we compute k -averages $\mathbf{E}^k \dots = \langle \dots \rangle_c$ over all stochastic variables $x = \mathbf{E}^m x_m$ being themselves averages over n_m microscopic variables x_m and compatible with the non-ergodicity constraint of the configuration c considered. Our task is to compute

$$v = \mathbf{E}^c v_c \text{ and } \Delta_{\text{ne}}^2 = \mathbf{V}^c v_c \text{ for } v_c \equiv \langle x^2 \rangle_c - \langle x \rangle_c^2. \quad (59)$$

We assume that the microscopic variables x_m are decorrelated as they come from uncorrelated microcells and set $v_{cm} \equiv \langle x_m^2 \rangle_c - \langle x_m \rangle_c^2$ for the variance of the microscopic variable x_m . Using the independence of the microcells m yields

$$v_c = \frac{1}{n_m} \times \left(\frac{1}{n_m} \sum_m v_{cm} \right) \quad (60)$$

$$\mathbf{V}^c v_c = \frac{1}{n_m^3} \times \left(\frac{1}{n_m} \sum_m \mathbf{V}^c v_{cm} \right) \quad (61)$$

where we have used that also the variances v_{cm} are independent stochastic variables. Note that the m -averages (brackets) do not depend on n_m for large n_m . Hence,

$$v = \mathbf{E}^c v_c \propto 1/n_m \text{ and } \Delta_{\text{ne}} \propto 1/n_m^{3/2}. \quad (62)$$

We have thus confirmed the exponents $\hat{\gamma}_{\text{int}} \equiv \gamma_{\text{int}} + 1 = 1$ and $\hat{\gamma}_{\text{ext}} \equiv \gamma_{\text{ext}} + 1 = 3/2$ stated in Sec. 2.4 for uncorrelated microscopic variables.

B Distribution of v_c

Since $\delta v_{\text{ext}}^2 = \mathbf{V}^c v_c$ is finite, the $v_c = \mathbf{E}^k v[\mathbf{x}_{ck}]$ of different configurations c must differ. It is useful to rewrite Eq. (20) by setting $v_c = v(1 + \delta_c)$ in terms of the “dimensionless dispersion” δ_c . Using $\mathbf{E}^c \delta_c = 0$ we have

$$(\delta v_{\text{ext}}/v)^2 \equiv s^2 = \mathbf{E}^c \delta_c^2 = \int d\delta_c p(\delta_c) \delta_c^2 \quad (63)$$

with s being the standard deviation of the normalized distribution $p(\delta_c)$. For a Gaussian distribution all moments are set by s . In general, however, $p(\delta_c)$ may be non-Gaussian and may depend on the preparation history. It may even happen in principle that some higher moments do not exist. We present in Fig. 10 the normalized distribution $p(x)$ for the rescaled dispersion $x = \delta_c/s$. A broad range of cases is considered. The histograms are obtained using the $n_c = 100$ independent configurations. A reasonable data collapse on the Gaussian distribution (bold solid line) is observed. This indicates that δv_{ext} or s are sufficient for the characterization of the distribution of the dispersion δ_c . The Gaussianity was also checked by means of the standard non-Gaussianity parameter [7], comparing the forth and the second moment of the distribution. Clearly, an even larger number n_c is warranted in future work for a more critical test of the tails of the distribution using a half-logarithmic representation.

References

1. W. Press, S. Teukolsky, W. Vetterling, B. Flannery, *Numerical Recipes in FORTRAN: the art of scientific computing* (Cambridge University Press, Cambridge, 1992)
2. N.G. van Kampen, *Stochastic processes in physics and chemistry* (North-Holland, Amsterdam, 1992)
3. T. Pang, *An Introduction to Computational Physics, 2nd Edition* (Cambridge University Press, Cambridge UK, 2006)
4. P.M. Chaikin, T.C. Lubensky, *Principles of condensed matter physics* (Cambridge University Press, 1995)
5. M. Doi, S.F. Edwards, *The Theory of Polymer Dynamics* (Clarendon Press, Oxford, 1986)
6. M. Rubinstein, R.H. Colby, *Polymer Physics* (Oxford University Press, Oxford, 2003)
7. J.P. Hansen, I.R. McDonald, *Theory of simple liquids* (Academic Press, New York, 2006), 3rd edition
8. J.D. Ferry, *Viscoelastic properties of polymers* (John Wiley & Sons, New York, 1980)
9. W.W. Graessley, *Polymeric Liquids & Networks: Dynamics and Rheology* (Garland Science, London and New York, 2008)
10. E.B. Tadmor, R.E. Miller, R.S. Elliot, *Continuum Mechanics and Thermodynamics* (Cambridge University Press, Cambridge, 2012)
11. E.B. Tadmor, R.E. Miller, *Modeling Materials* (Cambridge University Press, Cambridge, 2011)
12. M.P. Allen, D.J. Tildesley, *Computer Simulation of Liquids, 2nd Edition* (Oxford University Press, Oxford, 2017)
13. D.P. Landau, K. Binder, *A Guide to Monte Carlo Simulations in Statistical Physics* (Cambridge University Press, Cambridge, 2000)
14. L. Klochko, J. Baschnagel, J.P. Wittmer, A.N. Semenov, *J. Chem. Phys.* **151**, 054504 (2019)
15. G. George, L. Klochko, A. Semenov, J. Baschnagel, J.P. Wittmer, *EPJE* (2021)
16. I. Procaccia, C. Rainone, C.A.B.Z. Shor, M. Singh, *Phys. Rev. E* **93**, 063003 (2016)
17. J.P. Wittmer, I. Kriuchevskiy, A. Cavallo, H. Xu, J. Baschnagel, *Phys. Rev. E* **93**, 062611 (2016)

18. I. Kriuchevskiy, J.P. Wittmer, H. Meyer, J. Baschnagel, *Phys. Rev. Lett.* **119**, 147802 (2017)
19. I. Kriuchevskiy, J.P. Wittmer, H. Meyer, O. Benzerara, J. Baschnagel, *Phys. Rev. E* **97**, 012502 (2018)
20. G. George, I. Kriuchevskiy, H. Meyer, J. Baschnagel, J.P. Wittmer, *Phys. Rev. E* **98**, 062502 (2018)
21. J.P. Wittmer, H. Xu, P. Polińska, F. Weysser, J. Baschnagel, *J. Chem. Phys.* **138**, 12A533 (2013)
22. J.L. Lebowitz, J.K. Percus, L. Verlet, *Phys. Rev.* **153**, 250 (1967)
23. J.P. Wittmer, A. Tanguy, J.L. Barrat, L. Lewis, *Europhys. Lett.* **57**, 423 (2002)
24. A. Tanguy, J.P. Wittmer, F. Leonforte, J.L. Barrat, *Phys. Rev. B* **66**, 174205 (2002)
25. A. Ninarello, L. Berthier, D. Coslovich, *Phys. Rev. X* **7**, 021039 (2017)
26. S.J. Plimpton, *J. Comp. Phys.* **117**, 1 (1995)
27. J.P. Wittmer, H. Xu, J. Baschnagel, *Phys. Rev. E* **91**, 022107 (2015)
28. L. Klochko, J. Baschnagel, J.P. Wittmer, A.N. Semenov, *Soft Matter* **14**, 6835 (2018)
29. A. Heuer, *J. Phys.: Condens. Matter* **20**, 373101 (2008)
30. P. Charbonneau, J. Kurchan, G. Parisi, P. Urbani, F. Zamponi, *Nature Commun.* **5**, 3725 (2014)